doi:10.1016/j.jmb.2008.08.025 J. Mol. Biol. (2008) 383, 437–453

JMB

Available online at www.sciencedirect.com

ScienceDirect

ELSEVIER

Folding Mechanism of Reduced Cytochrome *c*: Equilibrium and Kinetic Properties in the Presence of Carbon Monoxide

Ramil F. Latypov[1], Kosuke Maki[1], Hong Cheng[1], Stanley D. Luck[1] and Heinrich Roder[1,2*]

[1]*Fox Chase Cancer Center, Philadelphia, PA 19111, USA*

[2]*Department of Biochemistry and Biophysics, University of Pennsylvania, Philadelphia, PA 19104, USA*

Received 3 June 2008; received in revised form 8 August 2008; accepted 13 August 2008
Available online 22 August 2008

Despite close structural similarity, the ferric and ferrous forms of cytochrome *c* differ greatly in terms of their ligand binding properties, stability, folding, and dynamics. The reduced heme iron binds diatomic ligands such as CO only under destabilizing conditions that promote weakening or disruption of native methionine–iron linkage. This makes CO a useful conformational probe for detecting partially structured states that cannot be observed in the absence of endogenous ligands. Heme absorbance, circular dichroism, and NMR were used to characterize the denaturant-induced unfolding equilibrium of ferrocytochrome *c* in the presence and in the absence of CO. In addition to the native state (N), which does not bind CO, and the unfolded CO complex (U-CO), a structurally distinct CO-bound form (M-CO) accumulates to high levels (~75% of the population) at intermediate guanidine HCl concentrations. Comparison of the unfolding transitions for different conformational probes reveals that M-CO is a compact state containing a native-like helical core and regions of local disorder in the segment containing the native Met80 ligand and adjacent loops. Kinetic measurements of CO binding and dissociation under native, partially denaturing, and fully unfolded conditions indicate that a state M that is structurally analogous to M-CO is populated even in the absence of CO. The binding energy of the CO ligand lowers the free energy of this high-energy state to such an extent that it accumulates even under mildly denaturing equilibrium conditions. The thermodynamic and kinetic parameters obtained in this study provide a fully self-consistent description of the linked unfolding/CO binding equilibria of reduced cytochrome *c*.

Edited by C. R. Matthews

Keywords: protein folding; denaturation; heme; ligand binding; NMR

Introduction

Metalloproteins often depend on their cofactor not only for function but also for efficient folding and stabilization of their native structure. For example, in the absence of heme, myoglobin folds into a marginally stable state lacking some of the native α-helices and tertiary interactions,[1] and cytochrome b_{562} assumes a dynamic molten-globule-like conformation.[2] An even more extreme case is cytochrome *c* (cyt *c*), which is initially synthesized as a largely disordered apoprotein[3,4] and folds into a stable globular structure only after covalent attachment of the heme.[5,6] These observations are not inconsistent with the notion that the native structure of a protein is encoded in its sequence, but suggest that the cofactor carries some of the information defining the native structure.

It has long been known that the heme and its axial ligands have a profound influence on the folding process of horse cyt *c*.[7–17] Similar findings have been

*Corresponding author. Fox Chase Cancer Center, 333 Cottman Ave., Philadelphia, PA 19111, USA.
E-mail address: roder@fccc.edu.

Present addresses: R. F. Latypov, Amgen, Inc., Seattle, WA 98119, USA; K. Maki, Department of Physics, Graduate School of Science, Nagoya University, Aichi 464-8602, Japan; S. D. Luck, DuPont Agricultural Biotechnology, Newark, DE 19714, USA.

Abbreviations used: cyt *c*, cytochrome *c*; GuHCl, guanidine HCl; Fe^{2+} cyt *c*, ferrocytochrome *c*; 1D, one-dimensional; HSQC, heteronuclear single-quantum correlation.

reported for *c*-type cytochromes from other species, including yeast and photosynthetic bacteria,[18,19] but we focus here on horse cyt *c*, which has been studied especially thoroughly. Under typical denaturing conditions [e.g., 6 M guanidine HCl (GuHCl), pH >4], one of the two axial heme ligands, the imidazole nitrogen of His18, remains bound to the heme iron due to the fact that the adjacent Cys17 is covalently bound to the heme. However, coordination of the second axial ligand, the sulfur of Met80, is inherently less stable and readily dissociates under partly or fully denaturing conditions. In unfolded cyt *c*, the vacant heme coordination site can bind alternative ligands, including extraneous ligands [such as imidazole or, in the case of the reduced (Fe^{2+}) form, carbon monoxide], as well as intramolecular ligands (such as His, Lys, or the amino terminus in their deprotonated states). Detailed studies of such ligand exchange reactions in both iron oxidation states have provided a rich source of information on the conformational propensities and dynamics of the denatured state of cyt *c*.[12,20–27] The predominant sixth iron ligand in the unfolded state of oxidized (Fe^{3+}) cyt *c* is His33,[28] which can become trapped during refolding and leads to accumulation of relatively long-lived (~100 ms) intermediate states that feature both native-like and nonnative structural features.[10,13,14]

Although the structures of the oxidized and reduced forms of mitochondrial cyt *c*—as determined by X-ray crystallography[29–31] or NMR[32–35]—are very similar, the two forms differ greatly in terms of stability, dynamics, and folding kinetics.[12,36–41] The dramatic stabilization of the protein upon reduction of the heme is not fully understood, but appears to be due to a combination of electrostatic effects (the reduced heme is electrically neutral, while the oxidized heme carries a net charge of +1), differential affinity of the heme iron for axial ligands between the native and the unfolded conformations in both oxidation states, and dynamic/entropic contributions. The fact that only nonnative forms of ferrocytochrome *c* (Fe^{2+} cyt *c*) bind a CO ligand with high affinity to form a photolabile ligand complex has opened unique opportunities for manipulating the conformational transitions of the protein and for probing its dynamics on the microsecond-to-millisecond time scale.[12,20,21,23,25,27,42,43] In their initial equilibrium characterization of Fe^{2+} cyt *c* in the presence of CO, Jones *et al.* had already noticed that this system does not undergo a simple two-state unfolding transition.[12] When observing the GuHCl-induced unfolding transition for Fe^{2+} cyt *c* at 40 °C using tryptophan fluorescence, they measured a midpoint concentration C_m=3.7 M (m=2.6 kcal mol^{-1} M^{-1}) in the presence of CO (1 atm, corresponding to ~1 mM CO in solution) and a midpoint concentration C_m=5.1 M (m=3.6 kcal mol^{-1} M^{-1}) in the absence of CO. These parameters indicate that addition of CO results in a nearly 9-kcal mol^{-1} decrease in the stability of native Fe^{2+} cyt *c*. A similar unfolding transition was observed using far-UV CD spectroscopy. However, changes in heme absorbance indicative of CO binding had already been observed between 1 and 3 M GuHCl, where the fluorescence and far-UV CD signals remain at their native levels.[12] This is a clear indication that the unfolding transition in the presence of CO cannot be adequately described in terms of a two-state mechanism.

Despite this earlier evidence for noncooperative behavior, Bhuyan and colleagues concluded that reduced cyt *c* undergoes a two-state unfolding transition, both in the presence and in the absence of CO, based on their equilibrium and stopped-flow studies of folding and unfolding.[40,41,44,45] In order to resolve this controversy, we further characterized the unfolding equilibrium of Fe^{2+} cyt *c* in the presence and in the absence of CO using optical techniques and NMR. The results provide clear evidence that, in addition to the native state (N), which does not bind CO, and to the unfolded CO complex (U-CO), a structurally distinct CO-bound form (M-CO) accumulates at intermediate denaturant concentrations. Based on its optical and NMR properties, M-CO is a folded state with a native-like helical core and regions of local disorder in the segment containing the native Met80 ligand and adjacent loops. Kinetic measurements of CO binding and dissociation under native and denaturing conditions confirm our hypothesis that a state M, which is structurally analogous to M-CO, is populated even in the absence of CO. Even though M does not accumulate to detectable levels at equilibrium, its presence can limit the rate constant of unfolding, giving rise to a downward curvature in the log(rate)-*versus*-[denaturant] plot at high denaturant concentration, similar to that previously observed for oxidized *c*-type cytochromes.[13,18,46] The binding energy of the CO ligand lowers the free energy of this transient intermediate to such an extent that it accumulates even under mildly denaturing equilibrium conditions. The thermodynamic and kinetic parameters obtained in this study provide a fully self-consistent description of the linked unfolding/CO binding equilibria of reduced cyt *c*.

Results and Discussion

Effect of CO binding on absorbance-detected and CD-detected unfolding transition

The changes in heme coordination that accompany unfolding and CO binding give rise to major changes in the heme absorption spectrum of cyt *c*.[12,41,47] Figure 1 shows the absorption spectra of horse Fe^{2+} cyt *c* in the folded and GuHCl–unfolded forms. Addition of CO to unfolded cyt *c* (U) results in a large increase in the extinction coefficient for Soret absorption, consistent with the formation of a hexacoordinate low-spin complex (U-CO), with CO displacing the native Met80 sulfur at the sixth iron coordination site (because of the covalent linkage of the heme *via* Cys14 and Cys17, the native His18 ligand remains bound to the fifth coordination site under the denaturing conditions used here[7]). To measure the effect of CO on the unfolding equili-

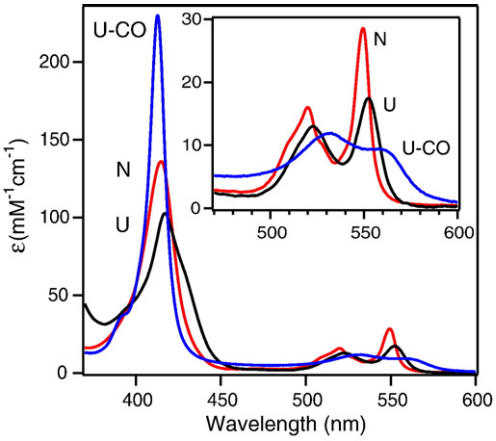

Fig. 1. Absorption spectra (Soret and visible regions) of horse Fe^{2+} cyt *c* at pH 7.0 (0.1 M sodium phosphate) and 20 °C under native conditions (red; N-state) and under denaturing conditions (6.5 M GuHCl), in the absence (black; U-state) and in the presence (blue; U-CO state) of 1 mM CO. The inset shows an expanded plot of the visible region (470–600 nm).

brium, we recorded absorbance spectra on a series of Fe^{2+} cyt *c* samples at different GuHCl concentrations equilibrated under 1 atm CO (~1 mM). Figure 2a shows the absorbance changes at selected wavelengths in the Soret region as a function of GuHCl concentration. At certain wavelengths (e.g., 410 nm), gradual changes in absorbance already occur at GuHCl concentrations between 1 and 2.7 M, while a single steeper transition centered around 3.6 M GuHCl is observed at other wavelengths (most pronounced at 418.5 nm). The two transitions are especially well resolved in the curve monitored at 416.5 nm, which shows two resolved phases with opposite signs, resulting in a bell-shaped curve. These observations provide clear evidence for the presence of an intermediate state with absorbance properties distinct from those of the equilibrium states populated at low (N) and high (U-CO) denaturant concentrations. The continuous lines in Fig. 2a were obtained by fitting a three-state mechanism (Scheme 1) to the transition curves measured at 0.5-nm intervals over the range from 380 to 430 nm, using global fitting procedures described by Latypov *et al.*[48] The equation used to describe Scheme 1 for global analysis involves a total of eight parameters: the global parameters C_{m1}, m_1, C_{m2}, and m_2 listed in Table 1 describe the two coupled denaturant-induced unfolding transitions, and the local parameters ε_N, $\varepsilon_{M\text{-}CO}$, $\varepsilon_{U\text{-}CO}$, and s_U describe the wavelength dependence of the data. A slope $s_U = d(\varepsilon_{U\text{-}CO})/dc$ was included to account for the effect of GuHCl on the absorbance of the fully unfolded CO complex. The spectral parameters ε_N, $\varepsilon_{M\text{-}CO}$, and $\varepsilon_{U\text{-}CO}$, plotted *versus* wavelength in Fig. 2b, represent the intrinsic absorption spectra of the three conformational states. ε_N is identical with the spectrum of the native state, while $\varepsilon_{U\text{-}CO}$ represents the spectrum of U-CO extrapolated to 0 M GuHCl, which is similar to the

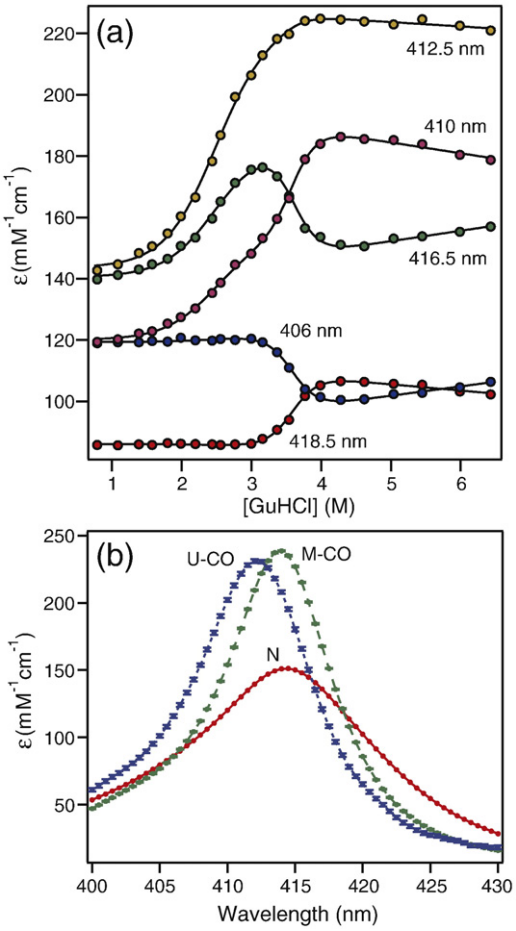

Fig. 2. (a) Absorbance changes at selected wavelengths in the Soret region associated with GuHCl-induced unfolding of Fe^{2+} cyt *c* (pH 7.0 and 20 °C) in the presence of 1 atm (~1 mM) CO. The lines represent a global fit of a three-state unfolding mechanism (Scheme 1) to the combined absorbance data (transition curves between 380 and 430 nm at every 0.5 nm). (b) Intrinsic Soret absorbance spectra of the N-, M-CO, and U-CO states obtained by plotting the respective extinction coefficients (local fitting parameters) *versus* wavelength.

spectrum of U-CO measured at high GuHCl concentrations (cf. Fig. 1). The Soret band of the M-CO state is more intense than those of both N and U-CO, and its absorption maximum (λ_{max}=413.5 nm) falls in between those of N (414.5 nm) and U-CO (412.5 nm).

The GuHCl-induced absorbance changes in the visible region of the spectrum (500–570 nm) were analyzed using the same procedure (see Supplementary Material). The native absorbance bands at 520 and 550 nm disappear gradually from 1 to 3.5 M GuHCl, reflecting primarily the transition from N to

$$\mathrm{N} \overset{K_{NM\text{-}CO}}{\rightleftharpoons} \mathrm{M\text{-}CO} \overset{K_{MU\text{-}CO}}{\rightleftharpoons} \mathrm{U\text{-}CO}$$

Scheme 1.

Table 1. Three-state equilibrium parameters for the GuHCl-induced unfolding transition of Fe^{2+} cyt *c* in the presence of 1 atm CO (pH 7 and 20 °C)

	C_m (M)	*m* (kcal mol^{-1} M^{-1})	ΔG (kcal mol^{-1})	ΔG_{NU} (kcal mol^{-1})
N ⇔ M-CO	2.487±0.004	1.604±0.015	3.99±0.04	15.3±0.3
M-CO ⇔ U-CO	3.559±0.003	3.179±0.047	11.3±0.2	

Equilibrium parameters were obtained by global fitting of heme absorbance data in the Soret region (380–430 nm), the visible bands at 520 and 550 nm, and the far-UV CD signal at 225 nm. Fitting also yielded the following spectroscopic properties for the M-CO intermediate: a Soret band at 413.5 nm with ε(413.5 nm) = 239 mM^{-1} cm^{-1}; a visible band with ε(550 nm) = 24.4 mM^{-1} cm^{-1} (87% of the native 550-nm band); and relative ellipticity at 225 nm equal to 0.2 (80% of the native far-UV CD signal).

M-CO. The spectrum of M-CO is close to that of U-CO, with a minor contribution of a native-like spectrum (cf. Fig. 1). We also used far-UV CD spectroscopy to monitor the denaturant-induced loss in the native helical secondary structure of reduced cyt *c* samples in the presence of CO. A plot of raw CD data (ellipticity at 225 nm) *versus* GuHCl concentration can be found in Supplementary Material. With increasing GuHCl concentration, the CD signal increases (becomes less negative) in two distinct steps, including a shoulder around 2.5 M accounting for ~20% of the total change and a sharp increase centered at 3.6 M GuHCl (in addition, there is a ~5% linear decrease between 0 and 1.5 M GuHCl). Initially, we used the equilibrium parameters (C_m and *m*-values) obtained by global fitting of the Soret absorbance data (Fig. 2) as constraints in fitting the visible heme absorption bands and ellipticity at 225 nm. The quality of the fits obtained (Supplementary Material) demonstrates the self-consistency of the data. The final set of thermodynamic parameters listed in Table 1 was obtained by globally fitting all of the available data, including the full absorbance spectra in the Soret region (380–430 nm), the visible bands at 520 and 550 nm, and the CD signal at 225 nm.

To compare the unfolding transitions monitored by different optical probes, we calculated normalized curves using the fitted intercepts and slopes of the native and U-CO states for each individual curve (Fig. 3a). The dispersion among the different curves reflects the fact that the relative contribution of the M-CO intermediate to the equilibrium transition is different for different optical parameters. For example, the absorbance at 412.5 nm (green squares) corresponds to an isosbestic point between the M-CO state and the U-CO state (Fig. 2b), and thus measures the gradual loss of the native population with increasing GuHCl concentration. In contrast, the curves at 406.5 nm (green uptriangles) and 418.5 nm (not shown) coincide with isosbestic points between N and M-CO (Fig. 2b), and thus reflect the population of the U-CO state, which builds up in a sharp transition centered at 3.6 M GuHCl. The ellipticity at 225 nm (diamonds) is dominated by a major transition at 3.6 M GuHCl with only minor changes (~20%) below 3 M, indicating that the M-CO state retains much of the native secondary structure, consistent with earlier reports.[12,41] In Fig. 3b, the populations of the three states derived from the global equilibrium parameters (Table 1) are plotted *versus* GuHCl concentration. M-CO reaches a maximum population of 73% at 3.3 M GuHCl. Also shown in Fig. 3a are normalized unfolding curves for reduced cyt *c* in the absence of CO measured in the Soret and visible regions of the absorption spectrum, as well as the CD signal at 225 nm. The fact that all optical probes can be fitted using a two-state model and can yield nearly identical equilibrium parameters confirms that unfolding of reduced cyt *c* is a cooperative process.[37,40] Global fitting of a two-state model to the optically

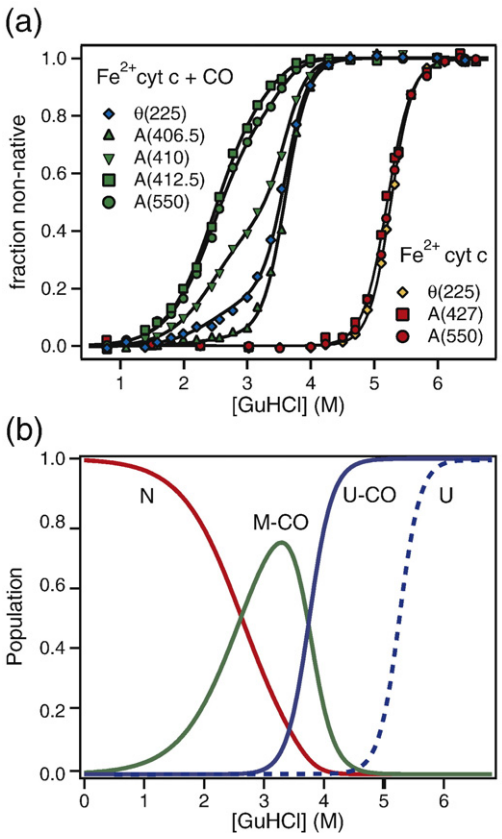

Fig. 3. (a) Normalized changes in ellipticity θ at 225 nm and heme absorbance at selected wavelengths *versus* GuHCl concentration for Fe^{2+} cyt *c* (pH 7.0 and 20 °C) in the presence of 1 mM CO (green and blue symbols) and in the absence of ligand (red and yellow symbols). (b) Relative populations of the three states (N: red; M-CO: green; U-CO: blue) populated during the unfolding of Fe^{2+} cyt *c* in the presence of CO, as predicted by equilibrium parameters in Table 1. The dashed line shows the population of the U-state accumulating during two-state unfolding in the absence of CO.

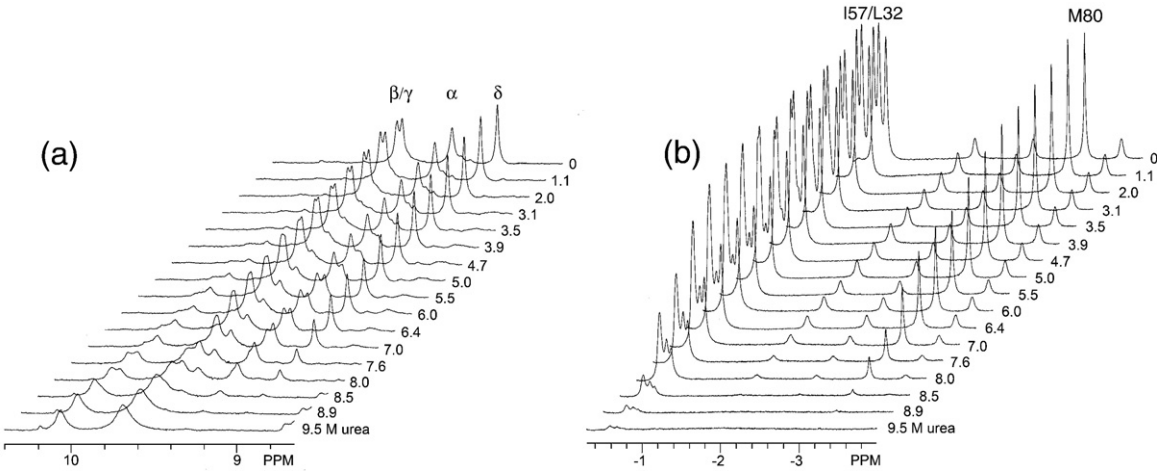

Fig. 4. One-dimensional NMR spectra of Fe^{2+} cyt *c* (pH 7.0, 22 °C) *versus* urea concentration. Expanded plots are shown for the low-field region containing heme *meso* protons (a) and for the high-field region containing methyl and M80 side-chain resonances (b).

monitored unfolding transitions of Fe^{2+} cyt *c* at 20 °C (in 0.1 M sodium phosphate, pH 7.0) yields an average midpoint $C_m = 5.22 \pm 0.06$ M and an *m*-value $m_{NU} = 3.25 \pm 0.24$ kcal $mol^{-1}M^{-1}$, corresponding to a free energy $\Delta G_{NU} = 17.0 \pm 1.3$ kcal mol^{-1}. Similar unfolding free energies (18.0–19.3 kcal mol^{-1}) have been reported previously for reduced cyt *c* under similar conditions.[49,50]

NMR-detected unfolding equilibrium

For a more detailed structural characterization of the unfolding equilibrium, we recorded a series of one-dimensional (1D) ^1H NMR spectra as a function of GuHCl or urea concentration on Fe^{2+} cyt *c* samples before and after the addition of CO (in D_2O with amide groups fully deuterated). Figure 4 shows representative spectra obtained *versus* urea concentration after equilibration with 1 atm CO. The resonances assigned to the Met80 side chain (Fig. 4b) begin to lose intensity at lower denaturant concentrations (>5 M urea) than the methyl resonances assigned to Leu32 and Ile57; the latter persists up to higher denaturant concentrations before disappearing over a narrow range of urea concentrations centered above 7 M (a similar behavior is seen for a number of other resolved resonances). These spectral changes clearly indicate that the native Met80–Fe coordination is disrupted at relatively low denaturant concentrations where the M-CO state is populated, while other regions of the protein become unfolded only at higher urea concentrations. Figure 4a shows the low-field region of the ^1H NMR spectrum, which contains resonances assigned to the four *meso* protons of the heme.[51] Although unambiguous assignments are available only for the native state, the complex urea-dependent spectral changes are clearly inconsistent with a cooperative (two-state) equilibrium. For example, the resonance assigned to the δ-*meso* proton in the N-state disappears at lower urea concentrations than the α-*meso* resonance, indicating that the former tracks the population of the N-

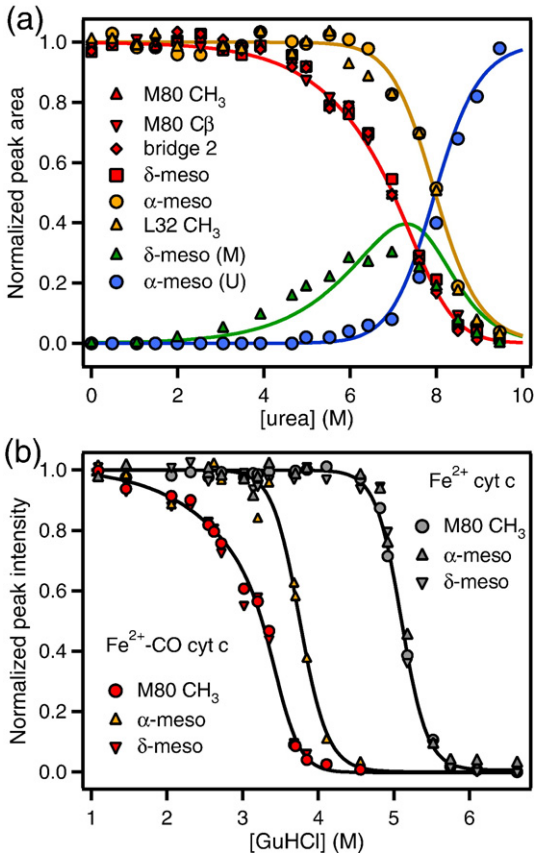

Fig. 5. (a) Normalized peak intensities of selected resonances resolved by 1D NMR (Fig. 4) *versus* urea concentration in CO-saturated D_2O solution. Red and yellow symbols indicate resolved peaks assigned to the N-state. Green triangles indicate the intensity of the peak at ~9.6 ppm due to the δ-*meso* proton in the M-state. Blue circles indicate the normalized intensity of the peak at 10.05 ppm assigned to the α-*meso* proton in the U-state. (b) Normalized peak intensities for the N-state resonances of the M80 methyl and two *meso* protons *versus* GuHCl concentration in the presence of 1 mM CO (colored symbols) and in the absence of ligand (gray symbols).

state while the latter reflects the combined populations of the N-state and the M-CO state. Another resonance near 9.6 ppm appears only at intermediate urea concentrations and shows the bell-shaped profile expected for the population of the M-CO state. Finally, two groups of resonances near 9.8 and 10.1 ppm, respectively, gain intensity at urea concentrations above 7 M and can thus be assigned to the fully unfolded state. For resolved resonances, normalized peak intensities were obtained by taking the ratio of the peak area between the spectra measured in the presence of CO and the spectra measured in the absence of CO, respectively (the latter shows no evidence for urea-induced unfolding up to the highest urea concentration measured; data not shown). A plot of relative peak intensities *versus* urea concentration (Fig. 5a) shows the behavior expected for a three-state unfolding equilibrium, including peaks assigned to the native state that disappear at relatively low urea concentrations (tracking the N-state; red symbols), others that persist up to higher denaturant concentrations (tracking the combined population of N and M-CO; yellow symbols), a third group that follows the population of the M-CO intermediate (green symbols), and a fourth group of lines that appears only at high denaturant concentrations where the U-CO state accumulates (blue symbols). The fact that the Met80 $C_\varepsilon H_3$ resonance is among the first to decay at low urea concentration confirms that the native Met80 ligand is displaced by the CO ligand. A corresponding set of ^{1}H NMR spectra was obtained for Fe^{2+} cyt *c* in the presence and in the absence of CO as a function of GuHCl concentration (data not shown for brevity; cf. Bhuyan[37]). The relative peak intensities of resolved N-state peaks *versus* GuHCl concentration show again a behavior characteristic of a three-state unfolding equilibrium (red and yellow symbols in Fig. 5b). Global analysis of the NMR data using Scheme 1 yields equilibrium parameters similar to those obtained by CD and absorbance (cf. Table 1). In contrast to urea, GuHCl is a denaturant that is sufficiently strong to reach the fully unfolded state even in the absence of CO (cf. Fig. 3). All of the resolved resonances in reduced cyt *c* decrease over a narrow range of GuDCl concentrations near 5 M (gray symbols in Fig. 5b), consistent with a fully cooperative (two-state) unfolding transition.[37,40]

NMR analysis of a metastable CO complex of Fe^{2+} cyt *c*

Although the CO ligand does not directly bind to the native state of reduced cyt *c*, a metastable CO complex is known to exist under native conditions.[25,37,41] To prepare this state, we initially equilibrate Fe^{2+} cyt *c* under 1 atm CO in the presence of 6 M GuHCl, forming the U-CO complex. The denaturant is then removed by gel filtration or its concentration is lowered by dilution, allowing the protein to refold, while the CO molecule remains tightly bound to the heme, preventing formation of the Met80 sulfur–Fe^{2+} bond. In the absence of light, the CO complex thus obtained (M-CO_{ms}) is metastable and corresponds to the M-CO equilibrium intermediate in the absence of denaturant. Thermal dissociation of the CO ligand occurs on a time scale of hours or longer at or below room temperature.[25,41] At 15 °C, the lifetime of the CO complex is about 4 h, which is sufficient to record a two-dimensional NMR spectrum on M-CO with minimal thermal dissociation of the ligand.

A uniformly ^{15}N-labeled recombinant H33N variant of horse cyt *c*[48,52–54] was initially prepared in the U-CO form by equilibrating a 1 mM solution of di-

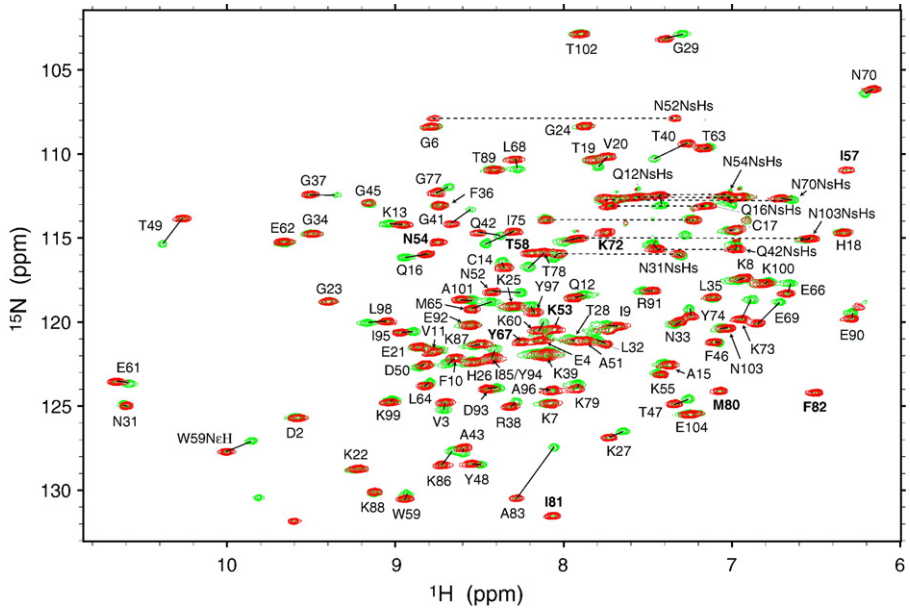

Fig. 6. ^{15}N–^{1}H HSQC spectra of native Fe^{2+} cyt *c* (red contours) and its metastable CO complex, M-CO_{ms} (green), recorded at 15 °C in 0.1 M sodium phosphate (pH 7.0). Cross-peaks labeled in bold undergo especially large CO-induced chemical shift changes and can be assigned only in the unligated form.

thionite-reduced protein under 1 atm CO in the presence of 6 M GuHCl (in 0.1 M phosphate buffer, pH 7). The denaturant was removed at 4 °C by passing the sample over a spinning gel-filtration column (Sephadex G25) equilibrated with buffer (0.1 M sodium phosphate in 95% H_2O/5% D_2O, pH 7.0). A ^{15}N–^{1}H heteronuclear single-quantum correlation (HSQC) spectrum was recorded at 15 °C. The spectrum of the M-CO_{ms} state thus obtained is shown in Fig. 6 (green contours) along with that of the N-state (red contours) recorded on the same sample after dissociation of the CO ligand (~8 h incubation at 15 °C). The spectrum of the refolded sample is virtually identical with that of a fresh Fe^{2+} cyt *c* sample that has never been unfolded and treated with CO. Backbone resonance assignments for the native reduced form were obtained using standard ^{15}N-based two-dimensional and three-dimensional NMR methods.[55–57] Our assignments (Fig. 6) are fully consistent with those reported by Liu *et al.*[54] The HSQC spectrum of M-CO_{ms} shows chemical shift dispersion and linewidths similar to those of the N-state, which is indicative of a tightly folded state. However, the spectra of the two forms show widespread differences, with a majority of residues experiencing significant chemical shift changes. Although independent resonance assignments for M-CO_{ms} cannot be obtained readily because of its metastable nature, many of the resolved cross-peaks can be assigned to nearby peaks in the native spectrum. In other cases, where an N-state peak has no obvious partner in the CO-bound form, we were able to obtain a lower-limit estimate for the chemical shift changes in each dimension from the distance to the nearest possible unassigned peak. In Fig. 7a, the normalized $^{1}H/^{15}N$ chemical shift changes (see figure caption) are plotted *versus* residue number. Arrows indicate residues for which only a lower-limit estimate is available. The largest concentration of residues undergoing major shift changes spans residues 80 through 85, with a second cluster in 50's. Other than a few isolated residues (40, 67, 72), only moderate chemical shift perturbations are observed throughout the remainder of the sequence, including the N-terminal segment up to residue 39 and the region containing the C-terminal α-helix (residues 87–104). In Fig. 7b, residues undergoing significant chemical shift changes upon CO binding are mapped onto the native cyt *c* structure. In this view, all of the perturbed residues are located on the left side of the structure, which contains the native Met80–heme linkage that is disrupted by competitive binding of a CO ligand.

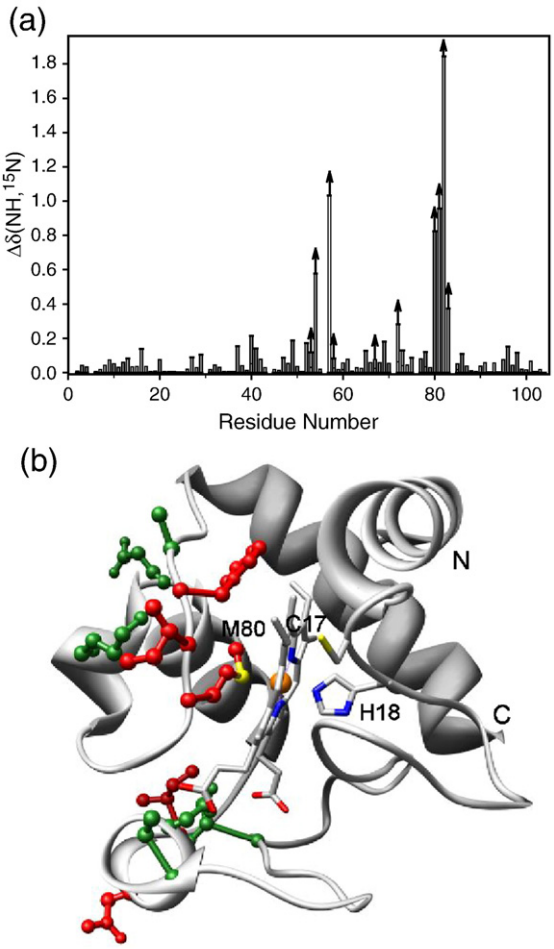

Fig. 7. (a) Chemical shift changes associated with dissociation of the CO ligand from M-CO_{ms} *versus* residue number. $^{1}H/^{15}N$ chemical shift changes were scaled as follows: $\Delta\delta(^{1}H,^{15}N) = \mathrm{sqrt}[\Delta\delta(^{1}H)^2 + (\Delta\delta(^{15}N)/10)^2]$, where $\Delta\delta(^{1}H)$ is the CO-induced change in the NH proton chemical shift and $\Delta\delta(^{15}N)$ is the corresponding change in the ^{15}N chemical shift. (b) Ribbon diagram of cyt *c* (Protein Data Bank code 1hrc) indicating regions of cyt *c* undergoing structural changes upon binding of a CO ligand under native conditions. Side chains shown in ball-and-stick mode indicate residues undergoing large chemical shift changes ($\Delta\delta > 0.4$ ppm; red) and intermediate changes ($0.15 \text{ ppm} \leq \Delta\delta \leq 0.4$ ppm; green).

Coupled CO binding/unfolding equilibria of Fe^{2+} cyt *c*

Our NMR evidence that M-CO_{ms} has a well-ordered structure distinct from that of the native state indicates that a substantial conformational change is required to allow binding of a CO ligand under nondenaturing conditions. This conclusion is consistent with the well-known fact that CO does not directly bind the native state of Fe^{2+} cyt *c*, unless it is destabilized in the presence of moderate concentrations of denaturant or extreme pH values.[12,58,59] Thus, we postulate that a native-like intermediate M exists even in the absence of CO. This hypothesis, which will be further justified below, leads to the following expanded scheme to describe the equilibrium between native, intermediate, and unfolded forms of cyt *c* and cyt *c*–CO (Scheme 2).

Equilibrium constants K_{NM}, K_{MU}, and $K_{MU\text{-}CO}$ describe conformational transitions, and K_a^M and K_a^U are second–order CO binding constants for the binding-competent intermediate and unfolded states,

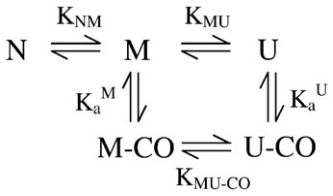

Scheme 2.

respectively. The fact that the equilibrium absorbance data in Fig. 2 and the NMR-detected unfolding transitions in Fig. 5 are well reproduced by a three-state mechanism (Scheme 1) indicates that the two unligated nonnative states in Scheme 2, M and U, are not populated at equilibrium in the presence of CO due to its high affinity for partially and fully unfolded states.

For a complete thermodynamic description of the coupled unfolding/ligand binding equilibrium of reduced cyt *c*, we need information on the binding constants of CO with the fully and partially unfolded states K_a^U and K_a^M. The former characterizes the U + CO ⇔ U-CO equilibrium and can be determined directly by measuring the heme absorbance changes as a function of CO concentration under fully denaturing conditions. Figure 8a shows the Soret region of the heme absorbance spectrum (1.2 μM sample of Fe^{2+} cyt *c* in 6.5 M GuHCl, pH 7.5 and 20 °C) recorded as a function of CO concentration ranging from 0 to 50 μM. Binding of a CO ligand to the sixth iron coordination site (His18 remains bound to the fifth position) is accompanied by a large increase in absorbance at 414 nm (A_{414}), which is plotted *versus* total CO concentration in Fig. 8b, using a log scale. The observation of a clear isosbestic point (at 418 nm) indicates that the assumption of a two-state binding equilibrium (U + CO ⇔ U-CO) is well justified. Least squares fitting of a 1:1 binding equilibrium (see Materials and Methods; Eq. (6)) accurately reproduces the data in Fig. 8b and yields a dissociation constant $K_d = 14 \pm 8$ nM. The relatively large error is due to the fact that reliable absorbance measurements can be obtained only at protein concentrations much higher than the dissociation constant, limiting the accuracy of the fit.

Rates of CO binding and dissociation from the unfolded state

The kinetics of the CO binding reaction with the GuHCl-denatured state of reduced cyt *c* (U + CO → U-CO) was measured by laser flash photolysis. The absorbance-detected kinetics was monitored at 550 nm following flash photolysis of unfolded Fe^{2+} cyt *c*–CO (in 6 M GuHCl), using a Nd–YAG laser to generate 8-ns pulses at 532 nm. The overall kinetics consists of three exponential phases and is fully consistent with previous studies in the Soret region.[12] The initial increase in absorbance with time constants $\tau_1 = 14$ μs and $\tau_2 = 0.4$ ms is attributed to the binding of Met65/Met80 and His26/His33, respectively.[12] The absorbance subsequently decreases with a rate that varies with CO concentration and is attributed to rebinding of the CO ligand to the heme. A plot of the rate of rebinding measured at 10 °C increases linearly as a function of CO concentration up to ~100 μM (Fig. 9a). The slope yields a second-order rate constant for CO binding of $1.76 \pm 0.08 \times 10^5$ M^{-1} s^{-1} (Table 2), which is comparable to the value reported for myoglobin (5×10^5 M^{-1} s^{-1})[60,61] but significantly lower than the CO binding rate of 2×10^8 to 4×10^8 M^{-1} s^{-1} found for model hemes in partially aqueous solvents.[62,63] The temperature dependence of the apparent CO binding rate (measured at a fixed CO concentration of 135 μM) shows Arrhenius behavior with a preexponential factor of 3×10^9 s^{-1} and activation energy $E_a = 11.2$ kcal mol^{-1} (Fig. 9b). This activation energy is more than twice the value for CO binding to myoglobin (5 kcal mol^{-1}).[60] The low second-order rate constant and large E_a observed in our case indicate that structural rearrangements at the

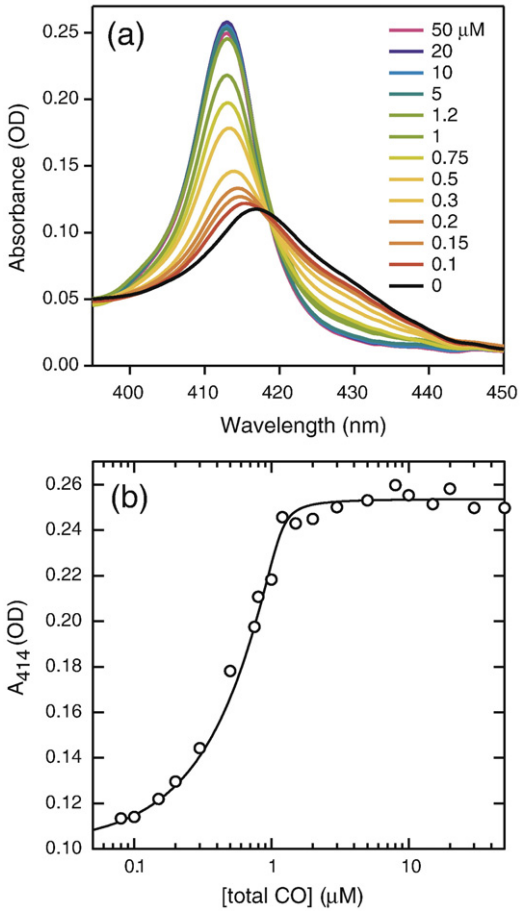

Fig. 8. (a) Absorbance spectra of Fe^{2+} cyt *c* in the Soret region as a function of total CO concentration ranging from 0 nM to 50 μM under unfolding conditions at 20 °C. The CO concentrations are color-coded as shown in the legend. The buffer contained 0.1 M Tris–HCl (pH 7.5), 6.5 M GuHCl, and 3 mM dithionite. (b) CO binding curve (circles) monitored by absorbance at 413 nm as a function of total CO concentration. The continuous line is a theoretical binding curve obtained by fitting the data to Eq. (6).

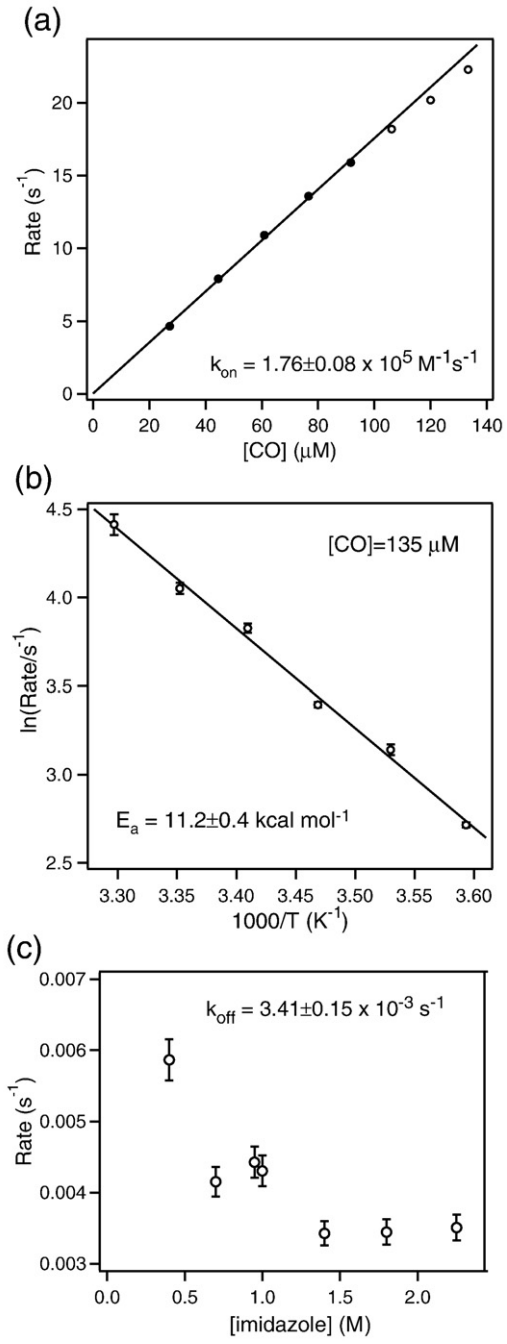

Fig. 9. (a) Rate constant of CO rebinding to unfolded Fe^{2+} cyt *c* (in 6 M GuHCl and 0.1 M sodium phosphate, pH 7.0) *versus* CO concentration measured at 10 °C by laser flash photolysis (see the text). (b) Arrhenius plot of the rate of CO recombination to unfolded Fe^{2+} cyt *c* measured by laser flash photolysis at variable temperatures (5–30 °C) and a constant CO concentration of 135 μM. (c) Rate constant for heme absorbance changes upon addition of imidazole to CO-bound Fe^{2+} cyt *c* (in 6.5 M GuHCl and 0.1 M Tris–HCl, pH 8.0) *versus* total imidazole concentration. The limiting value reached at high imidazole concentration represents the rate of CO dissociation.

heme, probably associated with the dissociation of nonnative His or Met ligands, are required to allow the binding of CO to unfolded Fe^{2+} cyt *c*.

The rate of CO dissociation from the fully unfolded U-CO state was measured by using imidazole as a competitive heme ligand. Both ligands share the sixth ligation site of the reduced heme iron, and when the U-CO (or M-CO) complex dissociates in the presence of a large excess of imidazole, an imidazole molecule rapidly occupies the open ligation site. Given the high solubility of imidazole, we can easily reach conditions where its rate of association is much faster than the CO dissociation rate. The rate-limiting step is then the dissociation of CO from the U-CO state, and the optically monitored kinetics yields the offrate for the CO ligand (k_{off}^{U}). The kinetics of CO dissociation was measured at 20 °C by monitoring the absorbance changes at the peak of the Soret band (413 nm) of U-CO in the presence of imidazole at concentrations ranging from 0.4 to 2.25 M imidazole. The reaction was initiated by a 2000-fold dilution of a CO-saturated solution of 1 mM Fe^{2+} cyt *c* containing 6.5 M GuHCl (0.1 M Tris–HCl, pH 8.0) with the same buffer containing imidazole. The dead time of manual mixing was approximately 30 s. The absorbance at 413 nm decays exponentially over a time period of about 30 min. Figure 9c shows that the observed rate initially decreases with increasing imidazole concentration and reaches a constant value of 3.41± 0.15×10^{-3} s^{-1} between 1.4 and 2.25 M.

Our kinetic data for the binding and dissociation of CO from the unfolded state of reduced cyt *c* are fully consistent with the equilibrium binding data in Fig. 8. Given the rate of CO binding to the U-state k_{on}^{U} measured by flash photolysis at 10 °C and the corresponding activation energy (Table 2), we estimate a value of 3.47×10^5 M^{-1} s^{-1} at 20 °C. Together with the U-CO dissociation rate k_{off}^{U}, measured by imidazole competition at 20 °C, we obtain an equilibrium dissociation constant $K_d^U = k_{off}^U/k_{on}^U$ of 10 nM, which agrees (within the error rate) with the value of 14±8 nM measured by equilibrium CO binding (Fig. 8).

Rates of CO binding and dissociation for the M-state

Because of the low population of the M-state in the absence of CO, the equilibrium constant for the M ⇔ M-CO transition and the rates of CO binding and dissociation with the M-state cannot be measured directly. However, the apparent rates of CO binding and dissociation are slow under conditions where the M-CO intermediate is the predominant nonnative equilibrium state (~1–3 M GuHCl) and can be measured by manual mixing. The CO binding rate at 2.5 M GuHCl (pH 7.0) was measured at temperatures ranging from 15 to 30 °C by monitoring the time-dependent absorbance changes in the Soret region (414 nm) following addition of CO. The reaction was initiated by manually mixing a Fe^{2+} cyt *c* stock solution in the absence of CO into a 50-fold-larger volume of CO-saturated buffer, yielding a final CO concentration near 1 mM. The observed kinetics is well represented by a single exponential

Table 2. Kinetic parameters for CO binding and dissociation of Fe^{2+} cyt *c*

Process	Measured rate constant	E_a (kcal mol^{-1})	Apparent rate at 20 °C (s^{-1}) (1 mM CO)
U+CO→U-CO	$1.76\pm0.08\times10^{5}$ M^{-1} s^{-1} (10 °C)	11.2±0.4	350
U-CO→U+CO	$3.41\pm0.15\times10^{-3}$ s^{-1} (20 °C)	–	3.4×10^{-3}
(N→M)+CO→M-CO	$2.0\pm0.1\times10^{-4}$ s^{-1} (20 °C)	30.3±1.8	2.0×10^{-4}
M-CO→M+CO	$3.1\pm0.5\times10^{-5}$ s^{-1} (10 °C)	26±3	1.5×10^{-4}

with an apparent rate $k_{app}=1.95\pm0.1\times10^{-4}$ s^{-1} at 20 °C. The observed kinetic amplitude accounts for the total absorbance change expected from equilibrium spectra in the absence and in the presence of CO, ruling out the presence of any rapid processes occurring during the dead time of this manual mixing experiment (~90 s). Figure 10a shows an Arrhenius plot of the observed rate of CO binding at 2.5 M GuHCl under CO-saturated conditions, yielding an activation energy of 30.3±1.8 kcal mol^{-1}.

To measure the rate of CO dissociation from the M-CO state populated at moderate denaturant concentrations, we first prepared U-CO in a CO-saturated solution containing 6 M GuHCl and generated the M-CO state by dilution with CO–free buffer to final GuHCl concentrations ranging from 0.075 to 4 M. Heme absorption spectra in the visible range (500–600 nm) were recorded at time intervals from 2 min to several hours after an 80-fold dilution of the U-CO sample with buffer. At early times, the spectrum is very similar to that of U-CO at equilibrium (cf. Fig. 1, inset), indicating that the CO ligand is still bound. The absorbance bands at 520 and 550 nm increase with time due to CO dissociation and formation of native cyt *c*. Our previous laser photolysis results indicate that the late folding event (M→N) triggered by dissociation of the trapped CO ligand occurs at a rate of ~1×10^{5} s^{-1}.[25] Thus, the kinetics observed at the low light levels used here is limited by thermal dissociation of the CO ligand rather than by photolysis or subsequent late-stage folding events. A logarithmic plot of the CO dissociation rate *versus* GuHCl concentration (Fig. 10b) shows that the rate remains nearly constant from 0 to 3.3 M GuHCl, followed by a sharp increase. The plateau corresponds to the region where M-CO accumulates with a negligible population of U-CO (Fig. 3b), and the observed rate (~3×10^{-5} s^{-1} at 10 °C; ~1.5×10^{-4} s^{-1} at 20 °C) represents that of a direct dissociation of the CO ligand from M-CO. The low denaturant dependence confirms that this process does not involve a major unfolding transition. Above 3 M GuHCl, where the concentration of U-CO increases sharply, the observed rate is increasingly determined by unfolding of M-CO, followed by dissociation from U-CO. To test this model further, we used numeric methods to solve the kinetic equations corresponding to Scheme 2, as described previously.[46] The continuous line in Fig. 10b represents the slowest observable rate constant (eigenvalue) predicted by the simulation, using the elementary rate constants shown as dashed lines. The fact that we can quantitatively reproduce the complex denaturant dependence of the observed rate for the coupled CO dissociation/unfolding process provides strong support for our model. The temperature dependence of the CO dissociation rate at low GuHCl concentrations (75 mM) shows Arrhenius behavior with an activation energy $E_a=26\pm3$ kcal

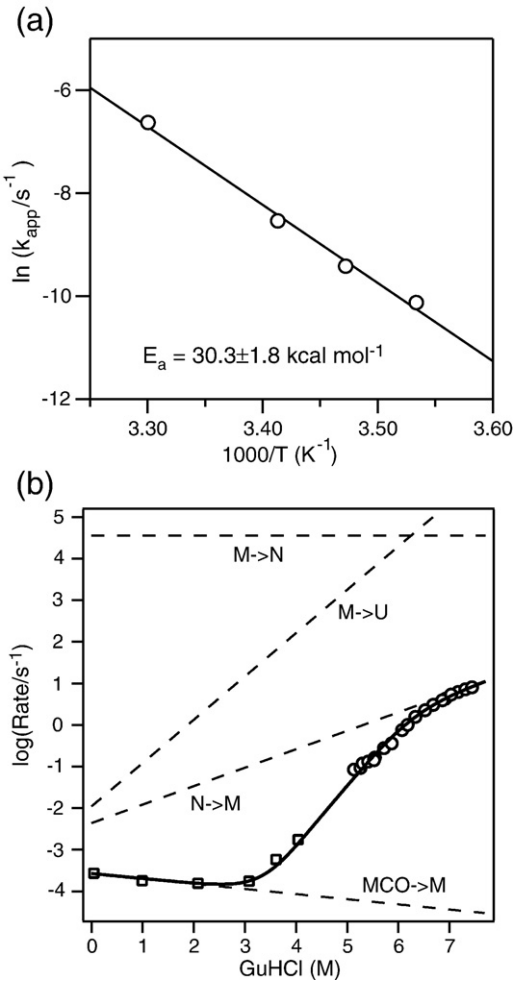

Fig. 10. (a) Arrhenius plot of the apparent rate of CO binding to Fe^{2+} cyt *c* at 2.5 M GuHCl [0.1 M sodium phosphate (pH 7.0) and 1 mM CO] measured by manual mixing. (b) Logarithmic plot of the rate constant of thermally activated CO dissociation from the metastable CO complex (M-CO_{ms}) *versus* GuHCl concentration (open squares). Also shown are the rate constants of unfolding of Fe^{2+} cyt *c* in the absence of CO (open circles) measured by absorbance-detected stopped-flow unfolding measurements at high GuHCl concentrations. The continuous line represents the observable rate constant for the coupled CO binding/unfolding process predicted based on Scheme 2. The dashed lines indicate the elementary rate constants used for kinetic modeling.

mol^{-1} (data not shown). The activation energy is similar to the value (23 kcal mol^{-1}) previously reported for Fe^{2+} cyt *c*-CO (pH 7.4) prepared by dilution from alkaline solution.[59] We and Yadaiah *et al.* have consistently observed a small decrease in dissociation rate between 0 and 3 M GuHCl, but the origin of this effect is not clear at this time (possible explanations include ionic strength and/or viscosity effects, in addition to local structure formation following CO dissociation).[43]

Comparison of the kinetic parameters for CO binding and dissociation at low and high denaturant concentrations (Table 2) reveals striking differences. Under stable conditions (<3 M GuHCl), where N and M-CO are the only equilibrium states populated in the absence and in the presence of CO, respectively, the apparent rate of CO binding is lower by a factor 2×10^6, and the activation energy is nearly threefold higher in comparison to the kinetics of CO binding to the unfolded state. Both observations indicate that the rate-limiting process for CO binding under these conditions involves a major conformational change in the protein rather than an intrinsic chemical barrier to binding.

According to Scheme 2, CO binding under nondenaturing conditions can be expressed in terms of the reaction mechanism in Scheme 3, where the rate constants k_{NM} and k_{MN} describe the structural transition between the N-state and the M-state, k_{on}^{M} is the second-order CO binding rate to the M-state, and k_{off}^{M} represents the corresponding dissociation rate. We already know one of the rate constants in this scheme, namely that of the late folding event $k_{MN}=8.3\times10^4\ s^{-1}$, which was measured by Pabit *et al.* in their flash photolysis experiments starting from the metastable M-CO_{ms} state.[25] Since the N ⇔ M equilibrium is strongly displaced towards N at low denaturant concentrations, we have $k_{MN}\gg k_{NM}$. Judging from the magnitude of the CO binding rate to U (Table 2), we also expect that $k_{MN}\gg k_{on}^{M}$. Under these conditions (analogous to hydrogen exchange in the EX_2 limit), the observed rate for CO binding k_{obs} can be approximated as:

$$k_{obs} = k_{NM}/k_{MN}k_{on} \qquad (1)$$

where k_{NM}/k_{MN} is the equilibrium constant for the N ⇔ M preequilibrium K_{NM}, and k_{on}^{M} is the apparent rate for CO binding to the M-state at a given CO concentration (e.g., 1 mM in a saturated solution at 1 atm). Since $K_{NM}\ll1$ under native conditions, Eq. (1) explains how the apparent rate of CO binding at low denaturant concentration can be very slow, even if the intrinsic CO binding rate to the M-state is relatively fast.

$$N \underset{k_{MN}}{\overset{k_{NM}}{\rightleftharpoons}} M \underset{k_{off}^{M}}{\overset{k_{on}^{M}}{\rightleftharpoons}} M\text{-}CO$$

Scheme 3.

Thermodynamic cycle

In the subsequent analysis, we make the plausible assumption that the intrinsic affinity of the U- and M-states is independent of denaturant concentration. While it is difficult to directly test this assumption because of the limited range of denaturant concentrations over which these states are populated, it is consistent with our data on the rate of CO dissociation from the M-state in Fig. 10b. For the cyclic portion of Scheme 2, the following free energy relationship holds:

$$\Delta G_{MU} + \Delta G_a^U - \Delta G_{MU-CO} - \Delta G_a^M = 0 \qquad (2)$$

From the CO binding/dissociation rates to the U-state (Table 2), we obtain $\Delta G_a^U = -RT\ \ln(k_{on}^U/k_{off}^U) = -6.7$ kcal mol^{-1}, and the equilibrium unfolding measurements in the presence of CO yield a value of 11.3 kcal mol^{-1} for $\Delta G_{MU\text{-}CO}$ (Table 1). Equation (2) thus reduces to

$$\Delta G_{MU} - \Delta G_a^M = 18\text{kcal mol}^{-1} \qquad (3)$$

The free energy for the N ⇔ M-CO transition provides an additional constraint:

$$\Delta G_{NM} + \Delta G_a^M = 4\text{kcal mol}^{-1}. \qquad (4)$$

By adding Eqs. (3) and (4), we obtain a value of 22 kcal mol^{-1} for the unfolding free energy in the absence of CO, $\Delta G_{NU} = \Delta G_{NM} + \Delta G_{MU}$. By comparison, the values for ΔG_{NU} obtained by two-state analysis of the reduced cyt *c* unfolding equilibrium (Fig. 3; cf. Bhuyan[49] and Bhuyan *et al.*[50]) range from 17.0 to 19.3 kcal mol^{-1}. This discrepancy is related, in part, to the unusually high midpoint for the GuHCl-induced unfolding transition of Fe^{2+} cyt *c* (5.2 M), which makes it difficult to define the post-transition baseline and introduces considerable uncertainty in ΔG due to long extrapolation, making the analysis highly sensitive to errors in the *m*-value. In contrast, our present estimate for ΔG_{NU} is based on more accurate thermodynamic parameters for the destabilized CO-bound form and reliable kinetic measurements for CO binding and dissociation. The total *m*-value measured in the presence of CO, $m_{NU} = m_{NM} + m_{MU} = 4.8$ kcal $mol^{-1}M^{-1}$ (Table 1), is above the range of values (3.3–3.7 kcal $mol^{-1}\ M^{-1}$) measured in the absence of CO (Fig. 3; Bhuyan[49]), suggesting that the latter is underestimated.

Kinetic evidence for accumulation of an unfolding intermediate

The available equilibrium data are insufficient for an independent determination of the free energies for all five transitions in Scheme 2. However, we were able to solve this problem by considering the kinetics of unfolding (a more detailed account of the kinetic mechanism of reduced cyt *c* will be presented elsewhere; Maki, Latypov, Hagen, and Roder, in preparation). The rate of unfolding of Fe^{2+} cyt *c* in the absence of CO, obtained by absorbance-detected

stopped-flow measurements under strongly denaturing conditions (5–7.5 M GuHCl), is included in Fig. 10b (open circles), along with elementary rate constants (dashed lines) and the predicted rate of unfolding (continuous line). The curvature in the chevron plot at high GuHCl concentrations can be explained as follows. Below 6 M GuHCl, the slope of the chevron plot is determined by k_{MU}, which represents a global unfolding transition and increases steeply with denaturant concentration. However, above 6 M GuHCl, the observed rate approaches k_{NM}, which becomes rate-limiting for unfolding under strongly denaturing conditions where $k_{MU} > k_{MN}$. Because the N→M transition is a local unfolding transition associated with the loss of the native Met80–heme linkage, the slope (kinetic *m*-value) associated with k_{NM} is lower than that associated with k_{MU}. Quantitative kinetic modeling of the data, using Scheme 1, fully reproduces the observed unfolding behavior (continuous line in Fig. 10b). The thermodynamic and kinetic parameters obtained are listed in Table 3. CO binding to the M- and U-states is expressed in terms of apparent rates and free energies at a CO concentration of 1 mM.

Bhuyan and Kumar previously observed a slight curvature in the unfolding rate of reduced cyt *c*, which they attributed to a denaturant-induced shift in the barrier position within the framework of a two-state model.[41,64] In contrast, we attribute the curvature in the unfolding branch of the chevron plot to a change in the rate-limiting barrier for unfolding due to the presence of a high-energy intermediate state. We previously proposed such a mechanism to describe the unfolding kinetics of oxidized cytochrome c_2, which shows a more pronounced rollover effect due to its lower stability.[46] Subsequent observations of nonlinear unfolding profiles for a number of proteins were also found to be consistent with a mechanism involving a high-energy unfolding intermediate.[65–67] Thus, the kinetics of unfolding we and others observed for reduced cyt *c* confirms the existence of state M in Scheme 1, which represents an obligatory unfolding intermediate both in the presence and in the absence of CO.

Table 3. Thermodynamic and kinetic parameters describing the unfolding and CO binding of Fe^{2+} cyt *c* in the absence of denaturant (pH 7 and 20 °C) predicted based on Scheme 2

Transition (states $i \Leftrightarrow j$)	Forward rate (s^{-1}) ($i \rightarrow j$)	Back rate (s^{-1}) ($j \rightarrow i$)	ΔG_{ij} (kcal mol^{-1})
N ⇔ M[a]	4.0×10^{-3}	8.3×10^{-4}	9.8
M ⇔ U[b]	–	–	12.2
M-CO ⇔ U-CO[b]	–	–	11.3
M ⇔ M-CO[c]	6.4	2.9×10^{-4}	−5.8
U ⇔ U-CO[c]	350	3.4×10^{-3}	−6.7

[a] The forward rate k_{NM} increases with GuHCl concentration (kinetic *m*-value m_{NM} = 0.6 kcal mol^{-1} M^{-1}), while the back rate k_{MN} is assumed to be independent of denaturant (see Pabit *et al.*[25]).

[b] Kinetic parameters describing the folding and unfolding transitions of Fe^{2+} cyt *c* in the presence and in the absence of CO will be reported elsewhere (Maki, Latypov, Hagen, and Roder, in preparation).

[c] The CO binding rates are apparent rate constants at 1 mM CO. CO binding and dissociation rates are independent of GuHCl concentrations, except for the M-CO→M+CO transition, which has a small negative *m*-value (−0.15 kcal mol^{-1} M^{-1}; Fig. 10b).

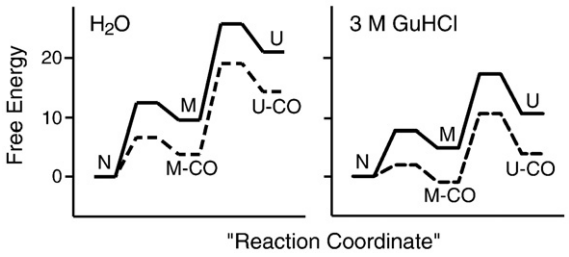

Fig. 11. Schematic free-energy diagrams for Fe^{2+} cyt *c* in the absence (solid lines) and in the presence (dashed lines) of CO under native conditions (left) and moderately denaturing conditions (right). The free energies of the various states and relative barrier heights are consistent with the equilibrium and kinetic parameters presented in Table 3, respectively.

Conclusions

The biological activity of cyt *c* as a mitochondrial electron transport shuttle critically depends on maintaining the native His/Met heme coordination,[68] and binding of alternative ligands is strongly disfavored under physiological conditions. However, CO and other exogenous ligands have such a strong affinity for binding 5-coordinate ferrous heme that they can displace the native methionine ligand under partially denaturing conditions. Our equilibrium and kinetic analyses of CO binding to unfolded Fe^{2+} cyt *c* (Figs. 8 and 9, Table 2) yield a dissociation constant of ~15 nM, which corresponds to a binding free energy of 6.7 kcal mol^{-1} at 1 mM CO. Thus, CO acts as a denaturant by dramatically lowering the free energy of nonnative conformations (those with weakened or disrupted sulfur–iron bond) relative to that of the native state. This made it possible to detect a structural intermediate, M, which is difficult to observe in the absence of exogenous ligand. As illustrated schematically in Fig. 11, in the absence of CO (continuous lines), M is a high-energy state that affects the kinetics of unfolding, but is not detectable at equilibrium. Addition of CO (dashed lines) lowers the free energy of M by nearly 6 kcal mol^{-1} (Table 3), making it observable as an equilibrium intermediate at moderate denaturant concentrations (Fig. 11, right). Our equilibrium unfolding measurements using optical probes (Figs. 2 and 3) and NMR (Figs. 4–6) provide unambiguous evidence for accumulation of a structural intermediate, M-CO, which has a tightly folded but nonnative conformation (Fig. 7). The structural and energetic properties of Fe^{2+} cyt *c*

in the presence of CO are in marked contrast to those of myoglobin, which binds diatomic ligands under native conditions and undergoes minimal structural rearrangement upon ligand binding.[69] Thus, we feel that the term "carbonmonoxycytochrome *c*" coined by Bhuyan and Kumar is misleading.[41]

Efforts to interpret the effect of CO on the unfolding transition of Fe^{2+} cyt *c* within a structural two-state framework (i.e., a cyclic scheme involving N, U, U-CO, and N-CO states)[41] have led to contradictions, or require the unsatisfactory assumption that the free energy for binding CO to the N-state is positive (unfavorable) at low denaturant concentrations and becomes negative with increasing GuHCl concentration. In contrast, our five-state mechanism (Scheme 2) provides a fully self-consistent thermodynamic description of the linked CO binding/unfolding equilibria of Fe^{2+} cyt *c* (Table 3, Fig. 11) and accounts for all of our equilibrium results and kinetic data on CO binding and dissociation under partly and fully denaturing conditions (Table 2). A key hypothesis underlying this analysis is that structurally equivalent intermediate states exist both in the presence and in the absence of the CO ligand (Scheme 2), which is supported by several lines of evidence: (i) NMR spectral differences (Fig. 6) indicate that displacement of Met80 by a CO ligand leads to widespread structural changes; (ii) the unfolding kinetics of Fe^{2+} cyt *c* is consistent with the presence of an obligatory unfolding intermediate, which limits the rate of unfolding at high GuHCl concentrations (Fig. 10); (iii) the free energy associated with the main structural unfolding transitions M ⇔ U in the absence of ligand (12.2 kcal mol^{-1}) is comparable to that obtained in the presence of CO (11.3 kcal mol^{-1}); and (iv) the M-state binds CO with similar affinity as the U-state, and the association/dissociation rates are only weakly dependent on denaturant concentration, as expected for a state with a largely exposed sixth heme coordination site (Table 3).

Accumulation of native-like states (late folding or early unfolding intermediates) appears to be a more general phenomenon. Equilibrium studies of oxidized cyt *c* using NMR, optical spectroscopy, and scattering methods have revealed a nonnative state that structurally resembles the M-CO state.[48,70,71,72] For both oxidation states, intermediates lacking the native Met80–iron linkage accumulate under moderately denaturing conditions. Binding of small-molecule ligands such as imidazole, cyanide, or azide to oxidized cyt *c* also results in some local unfolding of the structure on the distal (Met80) side of the heme and increased mobility.[73–75] The complex kinetics of unfolding observed for a number of proteins, including oxidized *c*-type cytochromes,[18,46,76] staphylococcal nuclease,[65] tendamistat,[66] and several other proteins,[67] has been interpreted in terms of mechanisms in which conversion of the native state into a high-energy intermediate can become a rate-limiting step for unfolding under strongly denaturing conditions.

Materials and Methods

Horse heart cyt *c* from Sigma-Aldrich Co. (St. Louis, MO) was used without further purification. GuHCl and urea were of ultrapure grade (MP Biomedicals, Solon, OH). All the other chemicals were of reagent grade. GuHCl concentration was determined by refractive index measurements using a Reichert–Jung refractometer (Leica, Bannockburn, IL). The concentration of oxidized cyt *c* was determined spectrophotometrically using an extinction coefficient of 1.06×10^5 $M^{-1}cm^{-1}$ at 410 nm. Protein solutions were equilibrated for a minimum of 30 min prior to measurement. Absorbance measurements were performed using a Perkin-Elmer or Hitachi spectrophotometer using 10- or 2-mm quartz cuvettes (0.5–25 μM cyt *c* solutions). The pH of the solutions was adjusted by addition of either HCl or NaOH and buffered with 0.1 M sodium phosphate (pH 7.0) or 0.1 M Tris–HCl (pH 7.5–8.0). Stock solutions of 1 M sodium dithionite were prepared in glass tubes with serum stoppers that were first purged with argon or nitrogen (highest purity available) to remove oxygen. Reduced (Fe^{2+}) cyt *c* was prepared by anaerobically adding dithionite to solutions of oxidized cyt *c* under an argon or nitrogen atmosphere. Dithionite concentrations were 0.5–5 mM for optical measurements and 5–20 mM for NMR experiments. All buffers and protein stock solutions were purged with oxygen-free argon, nitrogen, or CO gas in glass tubes or cuvettes sealed with serum rubber stoppers, and solutions were transferred using gas-tight Hamilton syringes.

CD measurements

The helix content of cyt *c* was measured at 225 nm with an Aviv 62DS spectropolarimeter using thermostatted cells with an optical path length of 2 mm. Ellipticity readings were time-averaged for up to 2 min at 60 points s^{-1}. The bandwidth was set to 2 nm, and the dynode voltage was kept below 400 V. The cyt *c* concentration was 25 μM. For the reduction of cyt *c*, the dithionite concentration was 0.5 mM; despite the significant dithionite absorbance, the CD signal was only slightly degraded. For CO binding, the air space that comprised about one-fourth of the total volume of the sample cell was filled with CO gas at 1 atm. CO samples were equilibrated for 30 min at 20 °C.

Equilibrium CO binding measurements

For measurement of the CO binding equilibrium with unfolded Fe^{2+} cyt *c*, CO concentrations were adjusted by mixing two buffers [0.1 M Tris–HCl (pH 7.5) containing 6.5 M GuHCl and 3 mM dithionite] saturated with CO (1.0 mM) and nitrogen, respectively, at atmospheric pressure. One-fifth volume of Fe^{2+} cyt *c* stock solution in the same buffer (purged with nitrogen before reduction) was added to a final protein concentration of 1.2 μM. Absorbance spectra in the Soret region (390-450 nm) were measured at 20 °C using a 1-nm bandwidth. The path length of the optical cuvette was 10 mm.

The dissociation constant (K_d) for the bimolecular reaction U-CO ⇔ U + CO is defined as:

$$K_d = \frac{[U][CO]}{[U-CO]} \quad (5)$$

where [U], [CO], and [U−CO] are concentrations of Fe^{2+} cyt *c* in the U-state, free CO, and unfolded CO complex,

respectively. Binding curves were obtained from the absorbance change at 414 nm ΔA_{414} corresponding to the maximum in the CO-bound form (Figs. 1 and 8a), using the following expression:

$$A_{414}([\mathrm{CO}]_{\mathrm{total}}) = A^0_{414} + \Delta A_{414} \times \frac{[\mathrm{CO}]_{\mathrm{total}} + C_0 + K_{\mathrm{d}}}{2C_0} \times \left(1 - \sqrt{1 - \frac{4C_0[\mathrm{CO}]_{\mathrm{total}}}{([\mathrm{CO}]_{\mathrm{total}} + C_0 + K_{\mathrm{d}})^2}}\right) \quad (6)$$

where A^0_{414} is the absorbance change in the absence of CO, $[\mathrm{CO}]_{\mathrm{total}}$ is the total CO concentration in solution, and C_0 is the protein concentration. Absorbance data were fitted to Eq. (6) using nonlinear least squares fitting.

Kinetics of CO binding and dissociation

Cyt *c* solutions were placed in thermostatted cells with path lengths of 0.2 cm for CO binding and 1 cm for CO dissociation. Temperature control was achieved by placing the cuvettes in a water-jacketed brass holder. Absorbance changes were monitored at 414 or 550 nm using light from a tungsten lamp. Absorbance changes due to thermal dissociation of CO were measured for up to 15 h. CO dissociation from the unfolded cyt *c* (U-CO) was measured in the presence of 0.4–2.25 M imidazole as a competitive ligand for the sixth iron coordination site. Fe^{2+} cyt *c* (1–2 mM) in a CO-saturated denaturing buffer (6.5 M GuHCl in 0.1 M Tris–HCl, pH 8.0) was diluted down to 0.5 μM protein in 1–3 ml of the same denaturing buffer in the absence of CO. For CO binding, the gas space of the cell was filled with 1 atm CO. For dissociation, 10 μl of 1 mM cyt *c*-CO in CO-saturated 6 M GuHCl was diluted with 0.5 ml of CO-free (pH 7.0) buffer (0.1 M sodium phosphate) to lower the GuHCl concentration. Interference from photolysis was minimized by using the smallest slit width (0.25 nm) for the monitoring light. From Arrhenius temperature dependence of observed rates, it was verified that photolysis due to the monitoring light is negligible. Solutions containing variable concentrations of CO were prepared by adding aliquots of a CO-saturated solution to argon- or nitrogen-saturated samples in air-tight cuvettes with less than 1 μl of gas space.

Laser flash photolysis experiments were performed using a nanosecond transient absorbance apparatus equipped with a Nd-YAG laser at the Regional Laser and Biotechnology Laboratories, University of Pennsylvania. Solutions of 2 μM Fe^{2+} cyt *c*-CO were placed in a thermostatted cuvette (1 cm×1 cm). Laser pulses were 8 ns in duration, with an energy of 150 μJ at 532 nm. Absorbance changes following photolysis were monitored at 550 nm.

Kinetic measurements of CO binding to the M-state were initiated by mixing a protein solution containing 125 μM cyt *c* in the absence of CO with a buffer saturated with CO using a gas-tight Hamilton syringe. The mixing ratio was 1:49 at a final protein concentration of 2.5 μM. The dead time of the mixing was approximately 90 s. Both solutions contained 0.1 M Tris–HCl (pH 7.5), 2.5 M GuHCl, and 5 mM dithionite. The protein stock solution and the buffer were purged with nitrogen and CO, respectively, before anaerobic addition of dithionite. The reaction was monitored by recording time-dependent changes in Soret absorbance at 414 nm on the spectrophotometer at temperatures ranging from 15 to 30 °C.

The kinetic traces for CO binding and dissociation were analyzed by nonlinear least squares fitting of a single-exponential function. The activation energies were determined using the Arrhenius relationship:

$$\ln(k_{\mathrm{obs}}) = \ln(A_0) - E_{\mathrm{a}}/(RT) \quad (7)$$

where R and T are the gas constant and absolute temperature, respectively. k_{obs}, A_0, and E_{a} are the observed binding/dissociation rate constant, preexponential factor, and activation energy, respectively.

NMR spectroscopy

For 1D NMR, labile amide protons were exchanged in D_2O in order to resolve the resonances of amide side-chain protons in the NH region of the NMR spectrum. A 0.5 mM cyt *c* solution in oxidized form (95%) prepared in 0.1 M phosphate (p*D* 10) D_2O buffer was incubated at 60 °C for an hour. Then the pH was adjusted to 7, and the solution was lyophilized. The concentration of urea (or GuHCl) was varied by mixing aliquots of pH 7 stock solutions of cyt *c* in D_2O buffer and 9.5 M urea (or 6.5 M GuHCl). 3-[Trimethylsilyl]propionic acid was also added as reference for NMR chemical shift. A stock solution of 1 M sodium dithionite was prepared in 0.1 M phosphate (p*D* 7) D_2O buffer. Cyt *c* was reduced anaerobically in NMR tubes by the injection of 10 μl of dithionite stock under continuous argon flow. The NMR tubes were tightly sealed with conical rubber stoppers. The dithionite reduction procedure caused no substantial change in denaturant concentration. For CO binding studies, sealed NMR tubes containing cyt *c* solution and 1 atm CO were shaken at room temperature (22 °C) for about 2 h to allow equilibration. NMR spectra were acquired on a Bruker DMX 600-MHz spectrometer. A typical spectrum was obtained by averaging 512 transients of 16,000 data points over a spectral width of 11.1 kHz. Multidimensional NMR spectra for a uniformly ^{15}N-labeled H33N variant of horse cyt *c* (details of the sample preparation are described in Latypov *et al.*[48]) were collected at 15 °C using a 5-mm *x,y,z*-shielded pulsed-field gradient triple-resonance probe. To confirm resonance assignments, ^{15}N-edited nuclear Overhauser effect-HSQC, total correlation-HSQC[56], HNHA[57], and HNHB[77] spectra were collected. ^{1}H/^{15}N HSQC experiments were run with 256 experiments in ^{15}N dimension (t_1) consisting of 40 scans and 4096 data points in ^{1}H dimension (t_2). Spectra processing and contour peak integration were performed using Felix (FelixNMR, San Diego, CA).

Acknowledgements

The work was supported by National Institute of Health grants R01 GM 056250 and CA06927, and an appropriation from the Commonwealth of Pennsylvania to the Institute for Cancer Research. We thank the Spectroscopy Support Facility at Fox Chase Cancer Center for maintaining the NMR and optical spectrometers, and the Regional Laser and Biotechnology Laboratory for access to nanosecond laser flash photolysis.

Supplementary Data

Supplementary data associated with this article can be found, in the online version, at doi:10.1016/j.jmb.2008.08.025

References

1. Lecomte, J. T., Sukits, S. F., Bhattacharya, S. & Falzone, C. J. (1999). Conformational properties of native sperm whale apomyoglobin in solution. *Protein Sci.* **8**, 1484–1491.
2. Feng, Y. Q., Wand, A. J. & Sligar, S. G. (1991). ^{1}H and ^{15}N NMR resonance assignments and preliminary structural characterization of *Escherichia coli* apocytochrome b_{562}. *Biochemistry*, **30**, 7711–7717.
3. Stellwagen, E., Rysavy, R. & Babul, G. (1972). The conformation of horse heart apocytochrome *c*. *J. Biol. Chem.* **247**, 8074–8077.
4. Fisher, W. R., Taniuchi, H. & Anfinsen, C. B. (1973). On the role of heme in the formation of the structure of cytochrome *c*. *J. Biol. Chem.* **248**, 3188–3195.
5. Dumont, M. E., Cardillo, T. S., Hayes, M. K. & Sherman, F. (1991). Role of cytochrome *c* heme lyase in mitochondrial import and accumulation of cytochrome *c* in *Saccharomyces cerevisiae*. *Mol. Cell Biol.* **11**, 5487–5496.
6. Gonzales, D. H. & Neupert, W. (1990). Biogenesis of mitochondrial *c*-type cytochromes. *J. Bioenerg. Biomembr.* **22**, 753–768.
7. Babul, J. & Stellwagen, E. (1972). Participation of the protein ligands in the folding of cytochrome *c*. *Biochemistry*, **11**, 1195–1200.
8. Brems, D. N. & Stellwagen, E. (1983). Manipulation of the observed kinetic phases in the refolding of denatured ferricytochromes *c*. *J. Biol. Chem.* **258**, 3655–3660.
9. Myer, Y. P. (1984). Ferricytochrome *c* refolding and methionine 80–sulfur linkage. *J. Biol. Chem.* **259**, 6127–6133.
10. Roder, H., Elöve, G. A. & Englander, S. W. (1988). Structural characterization of folding intermediates in cytochrome *c* by H-exchange labelling and proton NMR. *Nature*, **335**, 700–704.
11. Bhuyan, A. K., Elöve, G. A. & Roder, H. (1991). Redox effects on protein stability and folding kinetics of horse cytochrome *c*. *J. Cell Biochem.* **15G**, 188.
12. Jones, C. M., Henry, E. R., Hu, Y., Chan, C. K., Luck, S. D., Bhuyan, A. *et al.* (1993). Fast events in protein folding initiated by nanosecond laser photolysis. *Proc. Natl Acad. Sci. USA*, **90**, 11860–11864.
13. Elöve, G. A., Bhuyan, A. K. & Roder, H. (1994). Kinetic mechanism of cytochrome *c* folding: involvement of the heme and its ligands. *Biochemistry*, **33**, 6925–6935.
14. Sosnick, T. R., Mayne, L., Hiller, R. & Englander, S. W. (1994). The barriers in protein folding. *Nat. Struct. Biol.* **1**, 149–156.
15. Pascher, T., Chesick, J. P., Winkler, J. R. & Gray, H. B. (1996). Protein folding triggered by electron transfer. *Science*, **271**, 1558–1560.
16. Yeh, S. R., Takahashi, S., Fan, B. & Rousseau, D. L. (1997). Ligand exchange during cytochrome *c* folding. *Nat. Struct. Biol.* **4**, 51–56.
17. Telford, J. R., Tezcan, F. A., Gray, H. B. & Winkler, J. R. (1999). Role of ligand substitution in ferrocytochrome *c* folding. *Biochemistry*, **38**, 1944–1949.
18. Travaglini-Allocatelli, C., Gianni, S. & Brunori, M. (2004). A common folding mechanism in the cytochrome *c* family. *Trends Biochem. Sci.* **29**, 535–541.
19. Winkler, J. R. (2004). Cytochrome *c* folding dynamics. *Curr. Opin. Chem. Biol.* **8**, 169–174.
20. Hagen, S. J., Hofrichter, J., Szabo, A. & Eaton, W. A. (1996). Diffusion-limited contact formation in unfolded cytochrome *c*: estimating the maximum rate of protein folding. *Proc. Natl Acad. Sci. USA*, **93**, 11615–11617.
21. Goldbeck, R. A., Thomas, Y. G., Chen, E., Esquerra, R. M. & Kliger, D. S. (1999). Multiple pathways on a protein-folding energy landscape: kinetic evidence. *Proc. Natl Acad. Sci. USA*, **96**, 2782–2787.
22. Hammack, B. N., Smith, C. R. & Bowler, B. E. (2001). Denatured state thermodynamics: residual structure, chain stiffness and scaling factors. *J. Mol. Biol.* **311**, 1091–1104.
23. Hagen, S. J., Latypov, R. F., Dolgikh, D. A. & Roder, H. (2002). Rapid intrachain binding of histidine-26 and histidine-33 to heme in unfolded ferrocytochrome *C*. *Biochemistry*, **41**, 1372–1380.
24. Chang, I. J., Lee, J. C., Winkler, J. R. & Gray, H. B. (2003). The protein-folding speed limit: intrachain diffusion times set by electron-transfer rates in denatured $Ru(NH_3)_5$(His-33)–Zn–cytochrome *c*. *Proc. Natl Acad. Sci. USA*, **100**, 3838–3840.
25. Pabit, S. A., Roder, H. & Hagen, S. J. (2004). Internal friction controls the speed of protein folding from a compact configuration. *Biochemistry*, **43**, 12532–12538.
26. Kurchan, E., Roder, H. & Bowler, B. E. (2005). Kinetics of loop formation and breakage in the denatured state of iso-1-cytochrome *c*. *J. Mol. Biol.* **353**, 730–743.
27. Abel, C. J., Goldbeck, R. A., Latypov, R. F., Roder, H. & Kliger, D. S. (2007). Conformational equilibration time of unfolded protein chains and the folding speed limit. *Biochemistry*, **46**, 4090–4099.
28. Colón, W., Wakem, L. P., Sherman, F. & Roder, H. (1997). Identification of the predominant non-native histidine ligand in unfolded cytochrome *c*. *Biochemistry*, **36**, 12535–12541.
29. Takano, T. & Dickerson, R. E. (1981). Conformational change of cytochrome *c*: I. Ferrocytochrome *c* structure refined at 1.5 Å resolution. *J. Mol. Biol.* **153**, 79–94.
30. Takano, T. & Dickerson, R. E. (1981). Conformational change in cytochrome *c*: II. Ferricytochrome *c* refinement at 1.8 Å resolution and comparison with the ferrocytochrome structure. *J. Mol. Biol.* **153**, 95–115.
31. Berghuis, A. M. & Brayer, G. D. (1992). Oxidation state-dependent conformational changes in cytochrome *c*. *J. Mol. Biol.* **223**, 959–976.
32. Feng, Y., Roder, H. & Englander, S. W. (1990). Redox-dependent structure change and hyperfine nuclear magnetic resonance shifts in cytochrome *c*. *Biochemistry*, **29**, 3494–3504.
33. Gochin, M. & Roder, H. (1995). Protein structure refinement based on paramagnetic NMR shifts: applications to wild-type and mutant forms of cytochrome *c*. *Protein Sci.* **4**, 296–305.
34. Qi, P. X., Beckman, R. A. & Wand, A. J. (1996). Solution structure of horse heart ferricytochrome *c* and detection of redox-related structural changes by high-resolution ^{1}H NMR. *Biochemistry*, **35**, 12275–12286.
35. Banci, L., Bertini, I., Huber, J. G., Spyroulias, G. A. & Turano, P. (1999). Solution structure of reduced horse heart cytochrome *c*. *J. Biol. Inorg. Chem.* **4**, 21–31.
36. Gavish, B., Gratton, E. & Hardy, C. J. (1983). Adiabatic compressibility of globular proteins. *Proc. Natl Acad. Sci. USA*, **80**, 750–754.
37. Bhuyan, A. K. (1995). Oxidation state-dependent folding and stability of cytochrome *c*. Ph.D. Thesis, University of Pennsylvania.
38. Milne, J. S., Mayne, L., Roder, H., Wand, A. J. & Englander, S. W. (1998). Determinants of protein hydrogen exchange studied in equine cytochrome *c*. *Protein Sci.* **7**, 739–745.

39. Milne, J. S., Xu, Y., Mayne, L. C. & Englander, S. W. (1999). Experimental study of the protein folding landscape: unfolding reactions in cytochrome *c*. *J. Mol. Biol.* **290**, 811–822.
40. Bhuyan, A. K. & Udgaonkar, J. B. (2001). Folding of horse cytochrome *c* in the reduced state. *J. Mol. Biol.* **312**, 1135–1160.
41. Bhuyan, A. K. & Kumar, R. (2002). Kinetic barriers to the folding of horse cytochrome *C* in the reduced state. *Biochemistry*, **41**, 12821–12834.
42. Chen, E., Wood, M. J., Fink, A. L. & Kliger, D. S. (1998). Time-resolved circular dichroism studies of protein folding intermediates of cytochrome *c*. *Biochemistry*, **37**, 5589–5598.
43. Yadaiah, M., Kumar, R. & Bhuyan, A. K. (2007). Glassy dynamics in the folding landscape of cytochrome *c* detected by laser photolysis. *Biochemistry*, **46**, 2545–2551.
44. Prabhu, N. P., Kumar, R. & Bhuyan, A. K. (2004). Folding barrier in horse cytochrome *c*: support for a classical folding pathway. *J. Mol. Biol.* **337**, 195–208.
45. Kumar, R. & Bhuyan, A. K. (2005). Two-state folding of horse ferrocytochrome *c*: analyses of linear free energy relationship, chevron curvature, and stopped-flow burst relaxation kinetics. *Biochemistry*, **44**, 3024–3033.
46. Sauder, J. M., MacKenzie, N. E. & Roder, H. (1996). Kinetic mechanism of folding and unfolding of *Rhodobacter capsulatus* cytochrome c_2. *Biochemistry*, **35**, 16852–16862.
47. Butt, W. D. & Keilin, D. (1962). Absorption spectra and some other properties of cytochrome *c* and of its compounds with ligands. *Proc. R. Soc. London Ser. B.* **156**, 429–458.
48. Latypov, R. F., Cheng, H., Roder, N. A., Zhang, J. & Roder, H. (2006). Structural characterization of an equilibrium unfolding intermediate in cytochrome *c*. *J. Mol. Biol.* **357**, 1009–1025.
49. Bhuyan, A. K. (2002). Protein stabilization by urea and guanidine hydrochloride. *Biochemistry*, **41**, 13386–13394.
50. Bhuyan, A. K., Rao, D. K. & Prabhu, N. P. (2005). Protein folding in classical perspective: folding of horse cytochrome *c*. *Biochemistry*, **44**, 3034–3040.
51. Feng, Y. Q., Roder, H. & Englander, S. W. (1990). Assignment of paramagnetically shifted resonances in the ^{1}H NMR spectrum of horse ferricytochrome *c*. *Biophys. J.* **57**, 15–22.
52. Pollock, W. B. R., Rosell, F. I., Twitchett, M. B., Dumont, M. E. & Mauk, A. G. (1998). Bacterial expression of a mitochondrial cytochrome *c*. Trimethylation of Lys72 in yeast iso-1-cytochrome *c* and the alkaline conformational transition. *Biochemistry*, **37**, 6124–6131.
53. Dolgikh, D. A., Latypov, R. F., Abdullaev, Z. K., Colon, W., Roder, H. & Kirpichnikov, M. P. (1998). Expression of mutant horse cytochrome *c* genes in *Escherichia coli*. *Bioorg. Khim.* **24**, 756–759.
54. Liu, W., Rumbley, J., Englander, S. W. & Wand, A. J. (2003). Backbone and side-chain heteronuclear resonance assignments and hyperfine NMR shifts in horse cytochrome *c*. *Protein Sci.* **12**, 2104–2108.
55. Fesik, S. W. & Zuiderweg, E. R. (1990). Heteronuclear three-dimensional NMR spectroscopy of isotopically labelled biological macromolecules. *Q. Rev. Biophys.* **23**, 97–131.
56. Talluri, S. & Wagner, G. (1996). An optimized 3D NOESY-HSQC. *J. Magn. Reson.* **112**, 200–205.
57. Kuboniwa, H., Grzesiek, S., Delaglio, F. & Bax, A. (1994). Measurement of HN-H alpha *J* couplings in calcium-free calmodulin using new 2D and 3D water-flip-back methods. *J. Biomol. NMR*, **4**, 871–878.
58. Theorell, H. & Akesson, A. (1941). Studies on cytochrome *c*: III. Titration curves. *J. Am. Chem. Soc.* **63**, 1818–1827.
59. George, P. & Schejter, A. (1964). The reactivity of cytochrome *c* with iron-binding ligands. *J. Biol. Chem.* **239**, 1504–1508.
60. Austin, R. H., Beeson, K. W., Eisenstein, L., Frauenfelder, H. & Gunsalus, I. C. (1975). Dynamics of ligand binding to myoglobin. *Biochemistry*, **14**, 5355–5373.
61. Parkhurst, L. J. (1979). Hemoglobin and myoglobin ligand kinetics. *Annu. Rev. Phys. Chem.* **30**, 503–546.
62. Chang, C. K. & Traylor, T. G. (1975). Kinetics of oxygen and carbon monoxide binding to synthetic analogs of the myoglobin and hemoglobin active sites. *Proc. Natl Acad. Sci. USA*, **72**, 1166–1170.
63. Alberding, N., Austin, R. H., Chan, S. S., Eisenstein, L., Frauenfelder, H., Gunsalus, I. C. & Nordlund, T. M. (1976). Dynamics of carbon monoxide binding to protoheme. *J. Chem. Phys.* **65**, 4701–4711.
64. Oliveberg, M. (1998). Alternative explanations for "multistate" kinetics in protein folding: transient aggregation and changing transition-state ensembles. *Acc. Chem. Res.* **31**, 765–772.
65. Walkenhorst, W. F., Green, S. M. & Roder, H. (1997). Kinetic evidence for folding and unfolding intermediates in staphylococcal nuclease. *Biochemistry*, **63**, 5795–5805.
66. Bachmann, A. & Kiefhaber, T. (2001). Apparent two-state tendamistat folding is a sequential process along a defined route. *J. Mol. Biol.* **306**, 375–386.
67. Sanchez, I. E. & Kiefhaber, T. (2003). Evidence for sequential barriers and obligatory intermediates in apparent two-state protein folding. *J. Mol. Biol.* **325**, 367–376.
68. Moore, G. R. & Pettigrew, G. W. (1990). Cytochrome *c*: Evolutionary, Structural and Physiochemical Aspects Springer-Verlag, Berlin.
69. Brunori, M. (2000). Structural dynamics of myoglobin. *Biophys. Chem.* **86**, 221–230.
70. Russell, B. S., Melenkivitz, R. & Bren, K. L. (2000). NMR investigation of ferricytochrome *c* unfolding: detection of an equilibrium unfolding intermediate and residual structure in the denatured state. *Proc. Natl Acad. Sci. USA*, **97**, 8312–8317.
71. Russell, B. S. & Bren, K. L. (2002). Denaturant dependence of equilibrium unfolding intermediates and denatured state structure of horse ferricytochrome *c*. *J. Biol. Inorg. Chem.* **7**, 909–916.
72. Segel, D. J., Fink, A. L., Hodgson, K. O. & Doniach, S. (1998). Protein denaturation: a small-angle X-ray scattering study of the ensemble of unfolded states of cytochrome *c*. *Biochemistry*, **37**, 12443–12451.
73. Liu, G., Chen, Y., Shao, W., Lu, J. & Tang, W. (1997). The effects of imidazole binding on the conformation of cytochrome *c*. *Biochim. Biophys. Acta*, **1338**, 199–206.
74. Yao, Y., Qian, C., Ye, K., Wang, J., Bai, Z. & Tang, W. (2002). Solution structure of cyanoferricytochrome *c*: ligand-controlled conformational flexibility and electronic structure of the heme moiety. *J. Biol. Inorg. Chem.* **7**, 539–547.
75. Yao, Y., Wu, Y., Qian, C., Ye, K., Wang, J. & Tang, W. (2003). NMR study of the conformational transition of

cytochrome *c* upon the displacement of Met80 by exogenous ligand: structural and magnetic characterization of azidoferricytochrome *c*. *Biophys. Chem.* **103**, 13–23.
76. Gianni, S., Travaglini-Allocatelli, C., Cutruzzola, F., Brunori, M., Shastry, M. C. & Roder, H. (2003). Parallel pathways in cytochrome *c*(551) folding. *J. Mol. Biol.* **330**, 1145–1152.
77. Bax, A., Vuister, G., Grzesiek, S., Delaglio, F., Wang, A., Tschudin, R. & Zhu, G. (1994). Measurement of homo- and heteronuclear *J* couplings from quantitative *J* correlation. *Methods Enzymol.* **239**, 79–105.